Structural Safety and Reliability, Corotis et al. (eds), © 2001 Swets & Zeitlinger, ISBN 90 5809 197 X

Applications of remote sensing and GIS for damage assessment

F. Yamazaki
Earthquake Disaster Mitigation Research Center, NIED, Hyogo, Japan
Institute of Industrial Science, University of Tokyo, Tokyo, Japan

Keywords: remote sensing, GIS, damage assessment, aerial imagery, SAR, natural disasters

ABSTRACT: Remotely sensed imagery data from satellites and airborne platforms have become important tools to assess vulnerability of urban areas and to grasp damage distribution due to natural disasters. The platform and sensors of remote sensing should be selected considering the area to cover, urgency, weather and time conditions, and resolution of images. Satellites with optical and/or SAR sensors can cover much larger areas than other platforms, and hence, they can be used for macro-scale urban modeling and damage detection in large-scale natural disasters. Aerial television imagery and photography are very useful to observe buildings and infrastructures with high resolution. Thus automated detection of damage is possible using only post-event images or both pre- and post-event images. Use of airborne SAR is also highlighted for 3D urban modeling. In this paper, recent developments and applications of advanced technologies, notably, remote sensing and GIS, are reviewed from the viewpoint of risk assessment and post-event disaster management.

1 INTRODUCTION

In the last decade of the 20th century, although it was designated as the International Decade for Natural Disaster Reduction (IDNDR), a large number of devastating natural disasters attacked highly populated urban areas in the world, and a huge amount of human, structural, and socio-economic losses were brought due to them. Thus, vulnerability assessment before and after natural disasters has attracted significant attentions among researchers and practitioners of disaster management. In this regard, advanced technologies, notably remote sensing and GIS, have become important new tools in disaster management.

Recent advancements in remote sensing and its application technologies made it possible to use remotely sensed imagery data for assessing vulnerability of urban areas and for capturing damage distribution due to natural disasters (Shinozuka & Rejaie 2000). To obtain pre- and post-event information on built environment, several methods exist, such as field survey, aerial videography and photography, and satellite imagery. Figure 1 shows various platforms and sensors used for remote sensing. The platform and sensors should be selected considering the area to cover, urgency, resolution of images, and weather and time conditions. The first three items are closely related. If we want to get images over a large area, satellite imagery may be the most suitable tool although its resolution is in the order of several ten meters and return period is several weeks for commonly available earth observation satellites. On the contrary, aerial videography and photography from helicopters and light planes can be obtained much faster with higher resolution despite the fact that the area to cover is much small.

Regarding sensors on board platforms, synthetic aperture radar (SAR) can be used irrespective of sunlight and weather conditions, hence this feature is highly effective in damage surveys when optical remote sensing, such as multispectral scanning and aerial photography, is difficult. Massonnet et al. (1993) introduced interferometric SAR (IFSAR) analysis using phase information to estimate the distribution of ground displacement due to the 1992 Landars earthquake. Laser altimeter (LIDAR) is another new technique to profile 3D elevations of the earth surface (Gamba & Houshmand 2000).

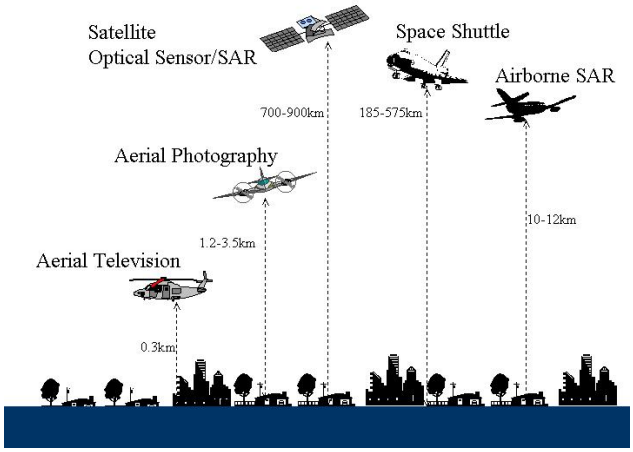

Figure 1. Platforms and sensors of satellite and airborne remote sensing.

Capability of optical/SAR satellite imagery has been demonstrated for damage detection in large-scale natural disasters. Using the pre- and post-event images of the 1995 Hyogoken-Nanbu (Kobe) earthquake observed by Landsat/TM, JERS/SAR, and ERS/SAR satellites, the areas with heavy building damage, fire and liquefaction were identified (Matsuoka & Yamazaki 1999, 2000a). In the study, the results of field surveys stored in GIS were employed as supervised learning data. Similar approaches comparing the pre- and post-disaster satellite images were carried out for the 1999 Kocaeli, Turkey earthquake (Estrada et al. 2000, Matsuoka & Yamazaki 2000b) and the 1990 Luzon, Philippine earthquake (Yamazaki & Matsuoka 1999). The satellite images together with GPS were also employed in a damage survey (Eguchi et al. 2000b) after the Kocaeli earthquake.

Airborne remote sensing is more suitable to obtain detailed inventory and to collect damage data of built environment. SAR imagery is one of the most promising techniques in this objective and a pioneer study on mathematical theory and image simulator has been conducted by Shinozuka et al. (2000). Interpretation of airborne SAR data was also attempted for the purpose of inventory development (Eguchi et al. 2000a) and urban modeling (Aoki et al. 1999). Although these investigations are still preliminary, airborne SAR imagery will be used for risk assessment and post-disaster damage detection of urban areas in the near future.

Aerial photography and videography from helicopters and light planes are practical and powerful tools to survey urban and suburban areas in pre- and post-event periods. Using aerial photographs, liquefaction induced permanent ground displacements were investigated for several damaging earthquakes in Japan (Hamada 1992, Hamada et al. 1995) and in the United Sates (O'Rourke at al. 1992, Sano et al. 1999). More recently, building damage due to the 1995 Kobe earthquake was interpreted visually using aerial photographs (Ogawa & Yamazaki 2000) and high-definition television (HDTV) images (Hasegawa et al. 2000a). Damage detection of buildings is further being developed to automated damage detection methods (Hasegawa et al. 2000b, Mitomi et al. 2000, 2001a, b) using the edge and color information of the post-earthquake images. Helicopters or light planes installing video and still cameras can provide damage information soon after the occurrence of a disaster. Hence such images are particularly useful in the early post-disaster damage detection as well as in the collection of inventory data in the ordinary period.

Use of GIS in disaster management has been accelerated in the last decade. Databases on built and natural environment have been developed on GIS platforms and damage assessments to natural disasters, especially urban earthquakes, have been conducted in many countries. One of the most enhanced damage databases has been developed for Kobe area after the 1995 Kobe earthquake and it has been used for the estimation of strong motion distribution (Yamaguchi & Yamazaki 2001) and for the construction of building fragility curves (Yamazaki & Murao 2000). GIS models are ex-

tensively utilized in real-time damage assessment systems (Yamazaki et al. 1994, 1998, Whitman et al. 1997, Shimizu et al. 2000).

In this paper, recent developments and applications of advanced technologies, notably, remote sensing and GIS, are reviewed from the viewpoint of risk assessment and disaster management. These technologies were born and developed in the different areas from "structural safety and reliability", but their application to our area is quite attractive and promising. Recent examples in the field of earthquake disaster mitigation are presented in the following.

2 SATELLITE REMOTE SENSING FOR DAMAGE DETECTION FROM THE 1995 KOBE EARTHQUAKE

2.1 *Damage Survey Data and Satellite Data*

Several satellites with optical sensors and/or SAR observed Kobe area before and after the Kobe earthquake on January 17, 1995. Since a part of the damage survey results is maintained as GIS data, a quantitative analysis on the surface changes in the damaged areas is possible. Liquefied areas were plotted on a GIS map based on the 1/50,000-scale ground-failure survey map (Hamada et al. 1995). The building damage data based on detailed survey results compiled by AIJ (the Architectural Institute of Japan) and CPIJ (the City Planning Institute of Japan), and digitized by BRI (Building Research Institute, Ministry of Construction) were utilized as the ground truth data (Fig. 2). In the GIS data, the building damage level was classified into five categories: damage by fire, severe damage, moderate damage, slight damage and no damage (BRI 1996).

We prepared several satellite images taken after the Kobe earthquake. Landsat/TM with optical sensors observed the area of interest on January 24, 1995, one week after the earthquake. We used the images taken on August 17, 1994 by Landsat for the data before the earthquake, and aimed to extract the change in the spectral characteristics of the damaged area. JERS/SAR image (Fig. 3) observed on February 5, 1995, 20 days after the Kobe earthquake, and five pre-event images were employed to examine the change in the backscattering characteristics of the area. SAR systems have the capability of recording complex signals including the amplitude (intensity) and phase of backscattered echoes from the objects on the earth's surface.

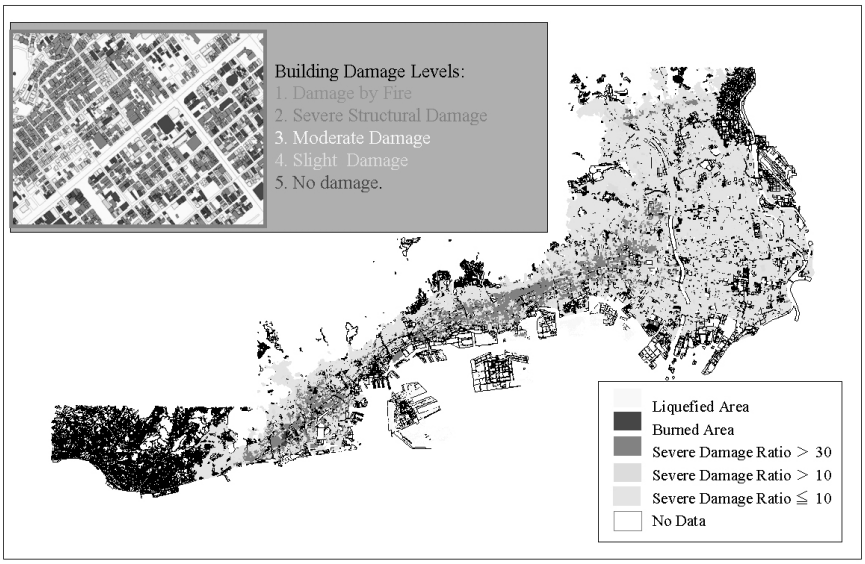

Figure 2. Building damage distribution due to the 1995 Kobe earthquake based on detailed survey results compiled by AIJ and CPIJ and digitized by BRI (BRI 1996)

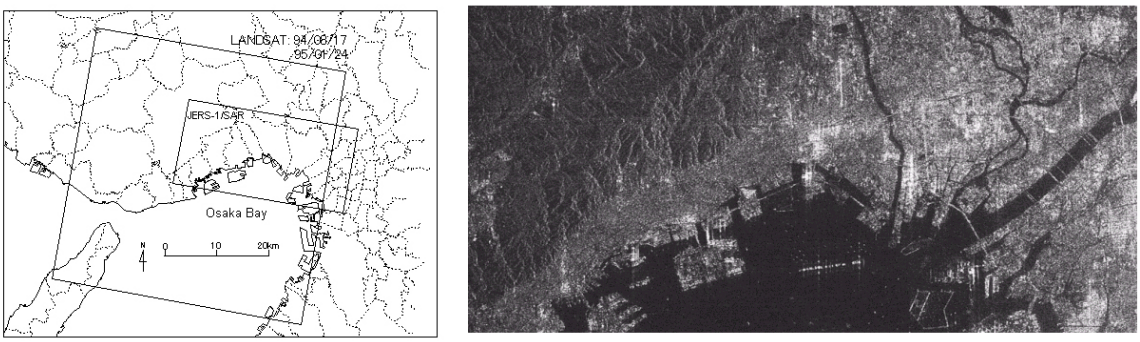

Figure 3. The area of the satellite images used in this study (left) and the backscattered intensity image of JERS/SAR taken after the Kobe earthquake (right).

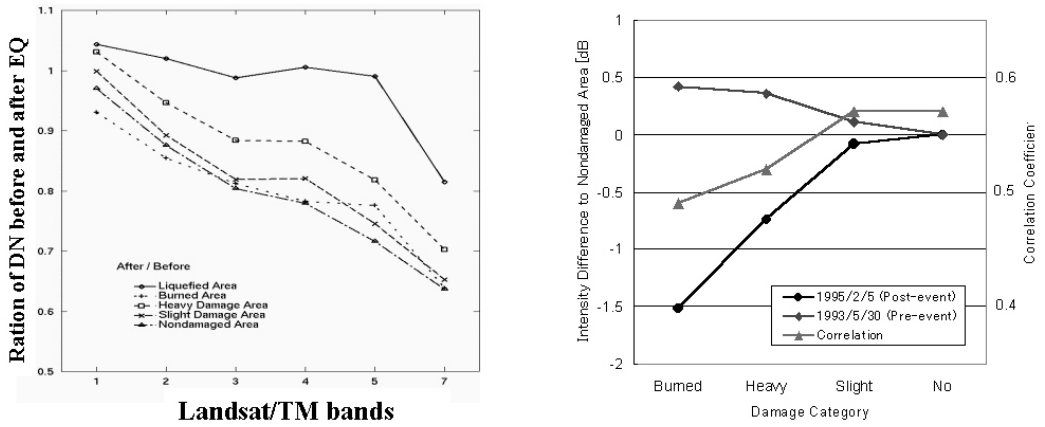

(a) (b)

Figure 4. (a) Ratio of digital numbers of Landsat/TM bands for the damaged areas before and after the earthquake and (b) comparison of backscattered intensity between the damaged and nondamaged areas and the correlation coefficient of JERS-1/SAR images taken before and after the earthquake.

2.2 *Characteristics of optical images*

Because the digitized values in the satellite images were different depending on the observation and surface conditions, digital number (DN) normalization is required before starting a study. The characteristics of the reflection of electromagnetic waves from the surface differ depending on the season because the sunlight and vegetation are different. One common technique to eliminate the seasonal difference is the band ratioing, which is defined as the ratio of the DN of each band to the DN of a reference band (Campbell 1996). We calculated the normalized DN (NDN) based on the band ratioing using band 6 as a reference band. The pre- and post-event images were registered after the affine geometric correction using ground control points. The correlation coefficients between the two sets of images were calculated using a 5 x 5 pixel window filter. Clouds and cloud shadows covering the area were removed using proper threshold values of several spectral bands. Areas with vegetation were also excluded from these images, based on the normalized difference vegetation index (NDVI). The pixels that represent the areas of liquefaction, fire, and heavy damage, slight damage and no damage of buildings were selected from the images to characterize the DN in the damaged areas.

The ratios of mean values of the NDN in the post-event and pre-event images for the classified damaged areas are shown in Fig. 4 (a). For the burned area, the ratio in the blue-light range of band

1 was especially low in comparison with the nondamaged area. These results are in good agreement with those of the damage survey performed by airborne multispectral scanner remote sensing (Mitomi & Takeuchi 1995). The ratio of the NDN in the liquefied area was high in the range from the visible to mid-infrared bands because of the higher reflectance of sand than the surface of asphalt. It is also conceivable that the ratio was raised in infrared bands in the heavy damage area due to the exposure of soil under walls and roofs upon the collapse of old wooden dwellings.

2.3 *Characteristics of SAR images*

The sets of two SAR images were overlain and the complex coherence was calculated for the area of the 7 x 7 pixel window around the initial position. Then matched positions were shifted pixel by pixel within the 15 x 15 pixel window to find the position at which the two images match best. By this procedure, the optimum pixel pair was determined at the position that yields the highest coherence and used to match all SAR images using the nearest neighbor transformation. The pixel pairs were also used as ground control points for the affine geometric correction to overlay SAR images with the damage survey data.

The coherence, which is the correlation calculated from the phases of the backscattering echoes of two co-registered complex SAR images, is a suitable and sensitive parameter for change detection and land-use classification. The complex coherence is usually adopted between two co-registered complex images acquired under slightly different geometrical configurations. However, decorrelated areas exist in the coherence image due to spatial and temporal decorrelation. The spatial decorrelation is resulted from the difference in the geometry of observation between two acquisitions, which is called baseline length *B*, shown in Fig. 5 (a). The temporal decorrelation is related to atmospheric effects such as moisture and surface changes in two acquisitions.

The pixels that represent the areas of fire, heavy damage, slight damage and no damage of buildings were selected from the SAR images. Although a slight influence of vegetation exists even in the SAR images, we disregarded it in this analysis. The trends of the mean values of intensity difference to the nondamaged area before and after the earthquake are shown in Fig. 4 (b). It is observed that the intensity values of the severely damaged area in the post-event image are smaller than those of the nondamaged area while such trend is not observed in the pre-event image. Generally, buildings show high reflectance because of the specular characteristics of the structure and ground surface (Fig. 5 (b)). Open spaces or damaged buildings have low reflectance because the microwaves are scattered in different directions. Following the earthquake, buildings were destroyed and in some cases, the debris was cleared leaving the ground exposed. Thus the intensity determined in the damaged areas is considered to be lower than that in the nondamaged areas. The mean values of the correlation coefficients between the pre- and post-event images for each damage class are also shown in the figure. A decreasing trend of the correlation coefficient with increasing the damage level is observed and it is coincidental with the difference of the backscattered intensities.

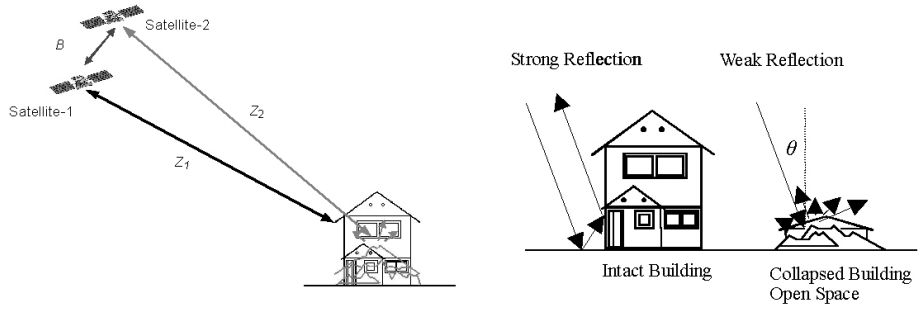

(a) (b)

Figure 5. (a) Basic principle of the repeat pass radar interferometry and (b) schematic diagram for surface objects and backscattered echoes.

3 CHARACTERISTICS OF AIRBORNE SAR IMAGES IN AN URBAN AREA

3.1 *CRL/NADSA airborne SAR and its images of Shinjuku, Tokyo*

Seismic risk in an urban area is closely related to the structure, material and dimension of buildings and their mutual distances. Hence it is important to study the plan, elevation and structure of buildings for evaluating seismic vulnerability of urban areas. Building inventory can be obtained by field surveys. However, a large amount of time and effort is required. Thus an easier method to develop building inventory is being sought. Airborne remote sensing can be an effective solution for the development of inventory since it can provide high-resolution images of the earth's surface and individual buildings can be identified in the images.

The Communications Research Laboratory (CRL), Japan and the National Space Development Agency of Japan (NASDA) have developed in collaboration an airborne high-resolution multiparameter SAR (Polarimetric and Interferometric SAR: PI-SAR). The airborne SAR is able to provide full-polarization information. The polarization characteristics are highly suitable for the identification of detailed surface conditions of objects because they differ according to the factors such as the building material and the density of city blocks. If we can identify the structures on the basis of their areas and heights from the polarization characteristics, the results can be used in seismic damage assessments. The relationship between the structures and the backscattering characteristics was investigated (Aoki et al. 1999) using airborne SAR data (CRL & NASDA 1999).

The PI-SAR observed a part of Tokyo Metropolitan area on September 30, 1997, and X-band full polarization data were acquired. The backscattering intensity images shown in Fig. 6 for a 3km x 3km area in Shinjyuku, a new city center of Tokyo, were used. Comparing the backscattering intensity images in the HH, HV, VH, and VV polarizations, the intensities of the co-polarization (HH, VV) were larger than those of the cross-polarization (HV, VH), and the HH polarization intensity was largest. High-rise buildings were indicated as a cause of strong backscattering reflection whereas low-rise buildings, forests and ponds in parks were found to have weak backscattering reflection.

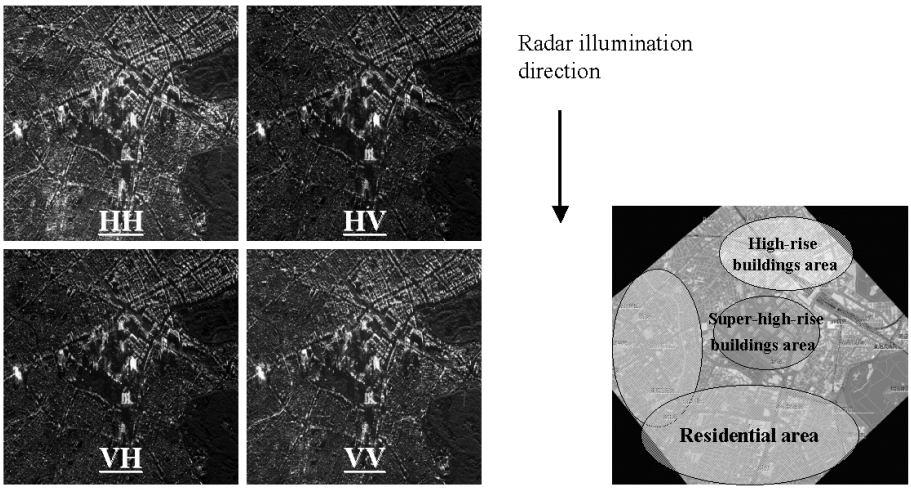

Figure 6. Backscattering intensity images of Shinjyuku, Tokyo by CRL/NASDA PI-SAR

3.2 *Polarization signature and polarized intensity*

The detailed polarization characteristics were investigated using the polarization signature of representative city blocks. These blocks labeled as max (R_{hh}), max (R_{vh}) and max (R_{vv}) were selected from the pixels having the maximum values of normalized polarization intensities. The details of wave polarization generation can be referred to Van Zyl et al. (1987) and Zebker (1987). The co-

and cross-polarized signatures of each extracted pixel are shown in Fig. 7. In the figure, the cross-polarized intensity for max (R_{hh}) is very low compared with the co-polarization intensity. As expected, the max (R_{hh}) area exhibited co- and cross-polarized signature shapes similar to those of the simple backscattering model from an object with a horizontal component. Thus it is estimated that the area of max (R_{hh}) have a scattering object normal to the radar illumination direction, which is a building along the street normal to the radar illumination direction. The entire polarized intensity for max (R_{vh}) is very low compared with those of max (R_{hh}) and max (R_{vv}). The area of max (R_{vh}) exhibited co- and cross-polarized signature shapes similar to those of the simple backscattering model from an object with a 45 degree inclined corner reflector component. The area of max (R_{vv}) showed co- and cross-polarized signature shapes similar to those of the simple backscattering model from an object with a vertical component. Since the R_{vv} value is high for tall buildings in the commercial area, the VV polarization intensity seems to have a relation with the building height.

The characteristics of the buildings in the studied area were examined by a field survey and aerial photographs. The actual structure at the max (R_{hh}) area was found to be a wooden house with a large wall almost normal to the radar illumination direction. The surrounding was a densely built-up residential district as seen by an aerial photograph shown in Fig. 8. The actual structure at the area of max (R_{vh}) was confirmed to be a low-rise building 45 degree inclined to the radar illumination direction. It is confirmed from the aerial photograph that this area is a residential district with the similar environment to that of the area of max (R_{hh}). The actual structure in the area of max (R_{vv}) is a super high-rise building. The surrounding area is a business district with many super high-rise buildings. Based on this study, it was found that the predominant polarization intensity differed with the height, shape, and alignment direction of buildings. A future study will be carried out to investigate the potential of polarimetric characteristics of airborne SAR for the development of building inventory.

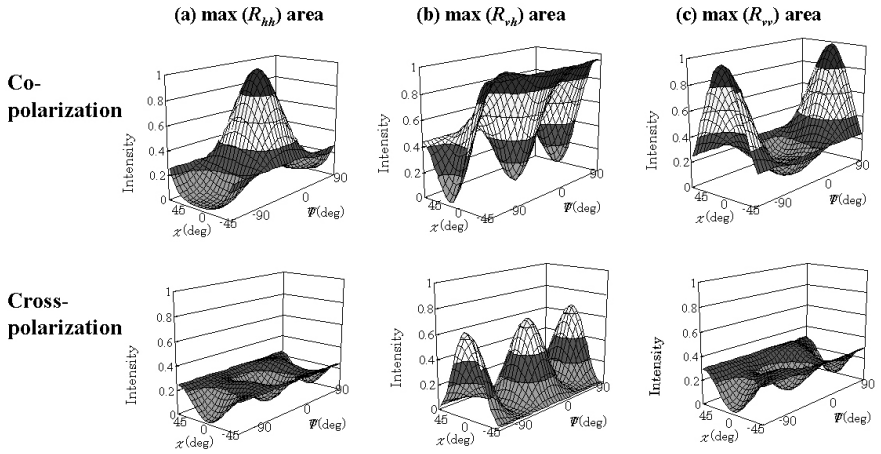

Figure 7. Polarization signatures for the three pixels with maximum polarized intensity.

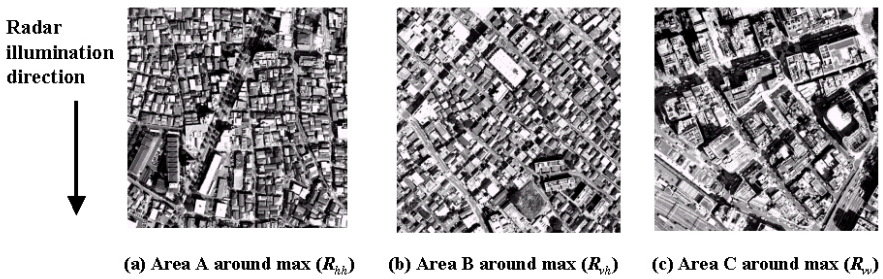

Figure 8. Aerial photographs of the surroundings of the selected areas in Figure 7.

4 AUTOMATED DAMAGE DETECTION OF BUILDINGS FROM AERIAL TELEVISION IMAGES AFTER NATURAL DISASTERS

4.1 *Use of aerial television images*

Airborne remote sensing is one of the promising techniques to capture damage information at an early stage of natural disasters. The present authors performed preliminary studies on the automated detection of building damage, and developed a method of automated damage detection based on only post-event images from the Kobe earthquake (Hasegawa et al. 2000b). The damage distribution estimated using the threshold values of color indices and edge elements (the multi-level slice method) agreed relatively well with the ground truth data. The method was also applied to the post-event images of the 1999 Kocaeli, Turkey and 1999 Chi-Chi, Taiwan earthquakes (Mitomi et al. 2000). Furthermore, an automated method of detecting areas with building damage based on the maximum likelihood classifier was devised (Mitomi et al. 2001a, b) in order to further improve the accuracy of automated damage detection. The results of automated detection of building damage from aerial images taken after the Gujarat, India earthquake are reported in the following.

4.2 *Aerial images of the 2001 Gujarat, India earthquake and automated damage detection*

In Gujarat Province, located in western India, numerous buildings were destroyed and more than 20,000 people were killed due the earthquake on January 26, 2001. A few members of Earthquake Disaster Mitigation Research Center conducted damage survey (EDM 2001) from the ground and air about two weeks after the earthquake (Fig. 9). In this investigation, digital images of damaged areas were taken with a digital video camera from a light plane. The plane took off from Ahmadabad, the largest city in Gujarat. After the plane flew from Ahmadabad to Bhuj by way of the northern route, it was refueled in Rajkot, located southeast of Bhuj. Then, the plane returned to Ahmadabad from Bhuj along the southern route. Figure 10 (a) shows a typical aerial image of building damage in Bhachau. The image has 640 pixels x 480 lines saved in the bitmap format.

Color indices and edge elements of image characteristics were used to identify severely damaged buildings. In the color indices, using image signals of the NTSC, which is one of the image transmitting systems for television, a tabular color system of RGB planes was transformed to the bare color system, HSI, which is close to the color perception of humans. Hue and saturation were derived by processing RGB components and brightness in order to remove the influence of sunshine on buildings. The median of a 7 x 7 pixel window in each HSI image was adopted as a representative value of each HSI component. The edge intensity, its variance and the uniformity of edge direction were derived using a Prewitt filter to detect the change in density among neighboring pixels. The six image characteristics (hue, saturation, brightness, edge intensity, its variance and the uniformity of the edge direction) were represented as raw eight-bit data.

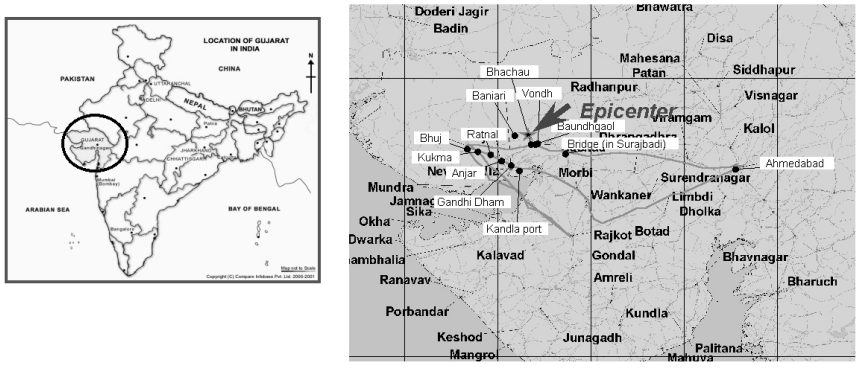

Figure 9. Aerial survey route by EDM for the damage due to the 2001 Gujarat, India earthquake.

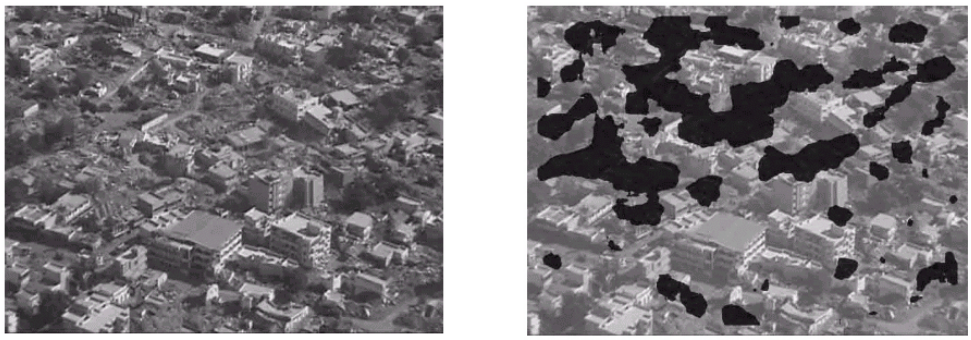

(a) (b)

Figure 10. (a) Aerial image of Bhachau for automated damage detection and (b) the extracted collapsed buildings by the multi-level slice method after spatial filtering.

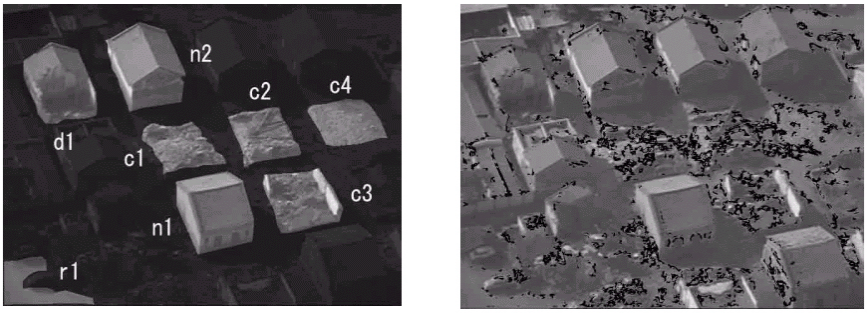

(a) (b)

Figure 11. (a) Training data for automated damage detection (c: collapsed buildings, d: damaged building, n: non-damaged buildings, r: asphalt road) and (b) the extracted pixels as damaged buildings from the image of Anjar.

Training data shown in Fig. 11 (a) were selected from the aerial image of a few houses in Anjar taken by the telephoto lens of the video camera. The cumulative relative frequency for each training datum was examined for each image characteristic, and the cumulative relative frequency of the training data was modeled by a line and the threshold value is determined for each image characteristic. Pixels within the ranges of all threshold values were regarded as corresponding to damage. Using only color indices, it was difficult to distinguish between severely damaged buildings and roads, however they could be distinguished using edge elements. The extraction result for Anjar is shown in Fig. 11 (b). Pixels of building debris were mostly extracted as damage. The extraction of pixels corresponding to building damage was also applied to aerial images of Bhachau and Bhuj using the threshold values for Anjar.

Then a spatial filtering operation was carried out to decrease surplus pixels and make it easy to identify the areas with building damage. The local density of the selected pixels was calculated by texture analysis. The window size corresponding to one building generally depended on factors such as the resolution of the image and built environment. A 31 x 31 pixel window was selected to be proportional to the scale of about one building in the aerial images and the result for Bhachau is shown in Fig. 10 (b). The result for the Bhachau image, which was obtained using the threshold values based on the Anjar image, seem to be close to the actual damage distribution. Although a good result was obtained in this example, it is suggested that threshold values for the image characteristics should be changed for each image or built environment because of the difference in some factors in each image, such as the influence of sunshine and built environment.

5 USE OF GIS FOR THE ESTIMATION OF SEISMIC GROUND MOTION IN THE KOBE EARTHQUAKE

In order to evaluate the structural damage in the area affected by earthquakes, it is important to estimate the distribution of earthquake ground motion. For the 1995 Kobe earthquake, several approaches have been conducted by a number of researches. As a method to estimate the intensity of seismic motion, e.g., the peak ground acceleration (PGA) and the peak ground velocity (PGV), the damages and effects to structures/objects are often used. Because the building damage was so extensive and several coordinated damage surveys were conducted after the Kobe earthquake, the building damage distribution might be most useful to estimate the detailed strong motion distribution in Kobe and neighboring cities (Yamaguchi & Yamazaki 2001).

Using the GIS database created by BRI (1996) and the seismic records, fragility curves as a function of PGA and PGV were developed and they were used to estimate the spatial distributions of PGA and PGV. From the strong motion records obtained in the earthquake, 17 free field records were selected. Some records were not used since the number of buildings around an observation point was not enough or severe liquefaction was reported around a recording site. To construct fragility curves for buildings, the building damage ratio around each observation point was calculated. The district block (corresponding to the postal address) where a reference seismometer is placed and its surrounding blocks were selected for the corresponding area of the seismometer. In selecting the surrounding blocks, the extent of damage and the soil condition were considered. Using the relationship between the damage ratio of low-storied residential buildings and the strong motion indices, the fragility curves were constructed by the least square method on the lognormal probability paper. Based on the obtained fragility curves and the building damage ratios in all the district blocks, the spatial distributions of the strong motion indices were back-calculated for the stricken area of the Kobe earthquake as shown in Fig. 12. The estimated strong motion distribution is consistent with the string motion data used and the reported seismic intensity distribution by the Japan Meteorological Agency (JMA 1997).

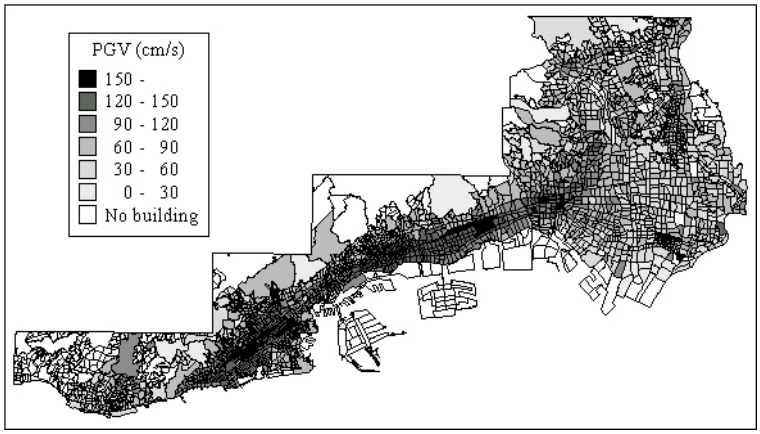

Figure 12. Distribution of the peak ground velocity (PGV) in the 1995 Kobe earthquake estimated from the damage ratio of low-storied residential buildings

6 CONCLUSIONS

Recent developments and applications of advanced technologies, notably, remote sensing and GIS, have been reviewed from the viewpoint of risk assessment and disaster management. Applications of these technologies in the field of "structural safety and reliability" are quite attractive and promising. Recent examples in the field of earthquake disaster mitigation were presented in this paper. Satellites with optical and/or SAR sensors can cover much larger areas than other platforms, and

hence, they can be used for macro-scale urban modeling and damage detection from large-scale natural disasters. Example of change detection using the pre- and post-event satellite images were shown for the 1995 Kobe earthquake. Aerial television imagery and photography are very useful to observe buildings and infrastructures with high resolution. Thus automated detection of damage is possible using only post-event images or both pre- and post-event images, and an example of building damage detection after the 2001 Gujarat, India earthquake was provided. Use of airborne SAR for the purpose of 3D urban modeling and application of GIS to evaluate seismic ground motion from building damage data were also demonstrated.

7 ACKNOWLEDGEMENT

The research outputs introduced in this paper have been produced by Dr. Masashi Matsuoka, Mr. Hirotada Hasegawa, Mr. Naoki Ogawa, Mr. Hisashi Aoki, Mr. Hijime Mitomi and Mr. Jun Saita of Earthquake Disaster Mitigation Research Center (EDM), and Dr. Naoya Yamaguchi of University of Tokyo. Their contributions are deeply appreciated.

REFERENCES

Aoki, H., Matsuoka, M. & Yamazaki, F., Uratsuka, S., Kobayashi, T. & Satake, M. 1999. Backscattering characteristics of airborne SAR images for seismic vulnerability assessment in urban areas: *Proceedings of the 20th Asian Conference on Remote Sensing*: 1: 115-120.

Building Research Institute 1996. *Final Report of Damage Survey of the 1995 Hyogoken-Nanbu Earthquake* (in Japanese).

Campbell, J. B. 1996. *Introduction to Remote Sensing*. Taylor & Francis.

Communications Research Laboratory & National Space Development Agency of Japan 1999. *Data set of CRL/NASDA SAR (PI-SAR)*: 1. CD-ROM.

Earthquake Disaster Mitigation Research Center: http://www.edm.bosai.go.jp/India2001/Survey1/1strec.html

Eguchi, R.T., Huyck, C.K., Houshmand, B., Tralli, D.M. & Shinozuka, M. 2000a. A new application for remotely sensed data: Construction of building inventories using synthetic aperture radar technology: *Proceedings of the Second Multi-lateral Workshop on Development of Earthquake and Tsunami Disaster Mitigation Technologies and Their Integration for the Asia-Pacific Region*: 217-228.

Eguchi, R.T., Huyck, C.K., Houshmand, B., Mansouri, B., Shinozuka, M. Yamazaki, F. & Matsuoka, M. 2000b. The Marmara Earthquake: A View from space: *The Marmara, Turkey Earthquake of August 17, 1999: Reconnaissance Report*. Technical Report MCEER-00-0001: 151-169.

Estrada, M., Matsuoka, M. & Yamazaki, F. 2000. Use of Landsat images for the identification of damage due to the 1999 Kocaeli, Turkey earthquake: *Proceedings of the 21st Asian Conference on Remote Sensing*. 2: 1185-1190.

Gamba, P. & Houshmand, B. Digital surface models and building extraction: A comparison of IFSAR and LIDAR data. *IEEE Transactions on International Geoscience and Remote Sensing*: 66 (7): 1959-1967.

Hamada, M. 1992. Large ground deformations and their effects on lifelines: 1964 Niigata Earthquake. *Case Studies of Liquefaction and Lifeline Performance During Past Earthquakes* 1: Technical Report NCEER-92-0001: 3:1-123.

Hamada, M., Isoyama, R. & Wakamatsu, K. 1995. *The 1995 Hyogoken-Nanbu (Kobe) Earthquake, Liquefaction, Ground Displacement, and Soil Condition in Hanshin Area*. Association for Development of Earthquake Prediction.

Hasegawa, H., Yamazaki, F., Matsuoka, M. & Sekimoto, I. 2000a. Extraction of building damage due to earthquakes using aerial television images. *Proceedings of 12th World Conference on Earthquake Engineering*: 8p. CD-ROM.

Hasegawa, H., Aoki, H., Yamazaki, F., Matsuoka, M. & Sekimoto, I. 2000b. Automated detection of damaged buildings using aerial HDTV images. *Proceedings of the IEEE 2000 International Geoscience and Remote Sensing Symposium*: 3p. CD-ROM: IEEE.

Japan Meteorological Agency 1997. Technical Report of the Japan Meteorological Agency: 119: *Report on the Hyogo-Ken-Nanbu Earthquake*, 1995 (in Japanese).

Massonnet, D., Rossi, M., Carmona, C., Adragna, F., Peltzer, G., Fiegl, K. & Rabaute, T. 1993. The displacement field of the Landars earthquake mapped by radar Interferometry. *Nature* 364: 138-142.

Matsuoka, M. & Yamazaki, F. 1999. Characteristics of satellite images of damaged areas due to the 1995 Kobe earthquake. *the Second Conference on the Applications of Remote Sensing and GIS for Disaster Management*: CD-ROM, The George Washington University.

Matsuoka, M. & Yamazaki, F. 2000a. Interferometric characterization of areas damaged by the 1995 Kobe earthquake using satellite SAR images. *Proceedings of the 12th World Conference on Earthquake Engineering*: 8p. CD-ROM.

Matsuoka, M. & Yamazaki, F. 2000b. Use of Interferometric satellite SAR for earthquake damage detection. *Proceedings of the 6th International Conference on Seismic Zonation*: 103-108. EERI.

Mitomi, Y. & Takeuchi, S. 1995. Analysis of spectral feature of the damaged areas by liquefaction and fire using airborne MSS data: *18th Japanese Conference on Remote Sensing*: 117-118 (in Japanese).

Mitomi, H., Yamazaki, F. & Matsuoka, M. 2000. Automated detection of building damage due to recent earthquakes using aerial television images. *Proceedings of the 21st Asian Conference on Remote Sensing*: 401-406.

Mitomi, H., Yamazaki, F. & Matsuoka, M. 2001a. Development of automated extraction method for building damage area based on maximum likelihood classifier: *Proceedings of the 8th International Conference on Structural Safety and Reliability*: 8p. CD-ROM.

Mitomi, H., Matsuoka, M., Yamazaki, F. & Saita, J. 2001b. Automated damage detection of buildings from aerial television images of the 2001 Gujarat, India earthquake: *Proceedings of the IEEE 2001 International Geoscience and Remote Sensing Symposium* 3p. CD-ROM: IEEE.

Ogawa, N. & Yamazaki, F. 2000. Photo-Interpretation of building damage due to earthquakes using aerial photographs. *Proceedings of the 12th World Conference on Earthquake Engineering*: 8p. CD-ROM.

O'Rourke, T.D., Roth, B.L. & Hamada, M. 1992. Large ground deformations and their effects on lifelines facilities: 1971 San Fernando Earthquake. *Case Studies of Liquefaction and Lifeline Performance During Past Earthquakes* 2: Technical Report NCEER-92-0002: 3:1-85.

Sano, Y., O'Rourke, T.D. & Hamada, M. 1999. Permanent ground deformation due to Northridge Earthquake in the vicinity of Van Norman Complex. *Proceeding of the 7th U.S.-Japan Workshop on Earthquake Resistant Design of Lifeline Facilities and Countermeasures Against Soil Liquefaction*: Technical Report MCEER-99-0019: 115-130.

Shimizu, Y., Watanabe, A., Koganemaru, K., Nakayama, W. & Yamazaki, F. 2000. Super high-density real-time disaster mitigation system. *Proceedings of the 12th World Conference on Earthquake Engineering*: 8. 7p. CD-ROM.

Shinozuka, M., Ghanem, R., Houshmand, B. & Mansouri, B. 2000. Damage detection in urban areas by SAR imagery. *Journal of Engineering Mechanics* 127 (7): 769-777, ASCE.

Shinozuka, M. & Rejaie, A. 2000. Correlational analysis of remotely sensed pre- and post-disaster images. *SPIE's 7th Annual International Symposium on Smart Structures and Materials*.

Van Zyl, J.J., Zebker, H.A. & Elachi, C. 1987. Imaging Radar Polarization Signatures: Theory and Observation: *Radio Science*: 22(4): 529-543.

Whitman, R.V., Anagnos, T, Kircher, C.A., Lagorio, H.J., Lawson, R.S. & Schneider, P. 1997. Development of a national earthquake loss estimation methodology: *Earthquake Spectra* 13(4): 643-661.

Yamazaki, F., Katayama, T. & Yoshikawa, Y. 1994. On-line damage assessment of city gas networks based on dense earthquake monitoring. *Proceedings of 5th U.S. National Conference on Earthquake Engineering* 4: 829-837.

Yamaguchi, N. & Yamazaki, F. 2001. Estimation of strong motion distribution in the 1995 Kobe earthquake based on building damage data: *Earthquake Engineering and Structural Dynamics* 30: 787-801.

Yamazaki. F, Noda, S & Meguro, K. 1998. Developments of early earthquake damage assessment systems in Japan. Structural Safety and Reliability: *Proceedings of the 7th International Conference on Structural Safety and Reliability*: 1573-1580.

Yamazaki, F. & Matsuoka, M. 1999. Remote sensing: Assessing the built environment by remote sensing technologies. *Second International Workshop on Earthquakes and Megacities*: 27-34.

Yamazaki, F. & Murao, O. 2000. Vulnerability functions for Japanese buildings based on damage data due to the 1995 Kobe Earthquake: *Implications of Recent Earthquakes on Seismic Risk. Series of Innovation in Structures and Construction* 2: 91-102. Imperial College Press.

Zebker, H.A., Van Zyl, J.J. & Held, D.N. 1987. Imaging radar polarimeter from wave synthesis: *Journal of Geophysical Research*: 92 (B1): 638-701.